

Crosstalk in microwave SQUID multiplexers

Cite as: Appl. Phys. Lett. **115**, 202601 (2019); <https://doi.org/10.1063/1.5116573>

Submitted: 27 July 2019 . Accepted: 26 October 2019 . Published Online: 15 November 2019

J. A. B. Mates , D. T. Becker , D. A. Bennett , B. J. Dober , J. D. Gard , G. C. Hilton , D. S. Swetz , L. R. Vale , and J. N. Ullom 



View Online



Export Citation



CrossMark

ARTICLES YOU MAY BE INTERESTED IN

[Selective terahertz emission due to electrically excited 2D plasmons in AlGaN/GaN heterostructure](#)

Journal of Applied Physics **126**, 183104 (2019); <https://doi.org/10.1063/1.5118771>

[Distributed optical fiber sensing: Review and perspective](#)

Applied Physics Reviews **6**, 041302 (2019); <https://doi.org/10.1063/1.5113955>

[Reduced nonradiative recombination in semipolar green-emitting III-N quantum wells with strain-reducing AlInN buffer layers](#)

Applied Physics Letters **115**, 202103 (2019); <https://doi.org/10.1063/1.5118853>

Lock-in Amplifiers
up to 600 MHz



Crosstalk in microwave SQUID multiplexers

Cite as: Appl. Phys. Lett. **115**, 202601 (2019); doi: 10.1063/1.5116573

Submitted: 27 July 2019 · Accepted: 26 October 2019 ·

Published Online: 15 November 2019



View Online



Export Citation



CrossMark

J. A. B. Mates,^{1,a)} D. T. Becker,¹ D. A. Bennett,² B. J. Dober,¹ J. D. Gard,¹ G. C. Hilton,² D. S. Swetz,² L. R. Vale,² and J. N. Ullom^{1,2}

AFFILIATIONS

¹Department of Physics, University of Colorado, Boulder, Colorado 80309, USA

²National Institute of Standards and Technology, Boulder, Colorado 80305, USA

a)john.mates@colorado.edu

ABSTRACT

Low-temperature detector technologies provide extraordinary sensitivity for applications ranging from precision measurements of the cosmic microwave background to high-resolution, high-rate x-ray, and γ -ray spectroscopy. To utilize this sensitivity, new instruments are being built, and new instruments are imagined, with ever greater pixel counts, but the scale of these instruments is limited by the capability of the readout electronics. Microwave SQUID multiplexing addresses the needs of these future instruments, exploiting gigahertz of bandwidths of coaxial cables and broadband components to combine hundreds to thousands of signals on a single readout line. A key feature of any multiplexer is the level of crosstalk between input channels. This crosstalk can degrade the sensitivity of the instrument, introduce systematic error, or simply confound data analysis. In this letter, we explain the primary mechanisms of crosstalk in a microwave SQUID multiplexer, calculate and measure their magnitude, and consider their effect and methods of mitigation.

<https://doi.org/10.1063/1.5116573>

Low-temperature detectors such as the superconducting Transition-Edge Sensor (TES)^{1,2} are sensitive devices for the measurement of incident power and energy, due to the low thermal fluctuations at the temperatures of operation (~ 100 mK). Since the noise of these detectors is typically less than the fluctuations of the signals they measure, scientific experiments have therefore assembled them into arrays of increasing size. This array size has been constrained by the capability to multiplex the signals onto a reasonable number of wires to carry the signals from cryogenic temperature to room temperature.

For example, while TES microcalorimeters routinely achieve record sensitivities for energy dispersive detectors at x-ray and gamma-ray wavelengths, the largest demonstrated arrays contain only ~ 250 detectors multiplexed using a time-division (TDM) basis set,^{3,4} and are read out using approximately 50 twisted-pairs. Other multiplexing techniques, such as frequency division multiplexing (FDM)⁵ and code-division multiplexing (CDM),⁶ have been used to read out arrays of similar scale.

Microwave techniques can expand the output bandwidth of the multiplexer from tens of megahertz to multiple gigahertz using coaxial cables and commercial broadband components. The microwave SQUID multiplexer⁷⁻⁹ uses rf-SQUIDs to modulate distinct superconducting microwave resonators, one for each input channel, coupled to a common microwave feedline. It has been demonstrated in various labs⁹⁻¹⁴ and is being applied to various experiments,^{12,15-18} with designs for bolometric applications with up to 2000 detectors per coax

and designs for calorimetric applications with 250 detectors per coax at 10 times the bandwidth per channel.

Crosstalk is a crucial parameter of any detector readout scheme: in bolometric measurements, it can produce spurious correlations between channels; in calorimetric measurements, it can produce a spurious background of low-energy events; in high-rate calorimetric measurements, the crosstalk between simultaneous events in different channels can degrade the energy resolution of both events. Multiplexer crosstalk has required some TES systems¹⁹ to restrict the count rate below the detector pileup limit in order to maintain energy sensitivity, partly negating the benefit of multiplexed arrays. Permissible crosstalk is highly sensitive

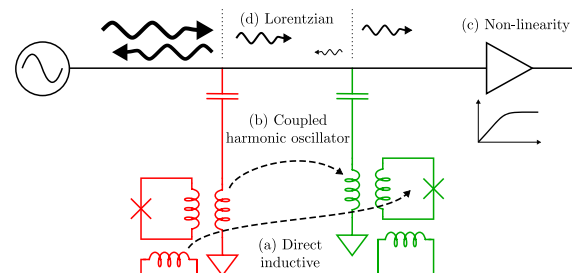


FIG. 1. Schematic of a two-channel microwave SQUID multiplexer indicating four mechanisms of crosstalk.

to the details of the application, such as the event rate, arrival statistics, ratio of signal to background events, and more, but we generally target <0.1% worst-case crosstalk and <0.01% on average.

This Letter will tour the known mechanisms of crosstalk in the microwave SQUID multiplexer (Fig. 1), starting from the obvious (a) direct inductive crosstalk, through the more subtle (b) coupled harmonic oscillator physics and (c) broadband nonlinearity, to the fundamental (d) crosstalk arising from the extended tails of the Lorentzian resonance shapes. It will throughout use the parameter χ to describe the fractional crosstalk of the modulation sideband of one microwave carrier, the “perpetrator,” into apparent modulation of another, the “victim.”

The most obvious mechanism of crosstalk to consider is that of parasitic inductive coupling of the input coil of one channel to the SQUID of a neighboring channel [Fig. 1(a)]. However, gradiometric design of the SQUIDs in these multiplexer circuits makes this mechanism negligible compared to the mechanisms we will discuss later.

We simulated in FastHenry the inductive couplings (Table I) for a representative NIST microwave SQUID multiplexer design. The direct inductive crosstalk from the nearest-neighbor input coil in this design is less than 0.02% and that from the next-nearest-neighbor is less than 0.01%. The coupling from one resonator to a neighboring SQUID is fractionally larger, but its contribution to crosstalk is less because the resonance frequency shift scales as the square of the inductive coupling.

However, the weak coupling between the resonators themselves [Fig. 1(b), Table I] can still provide a mechanism for substantial crosstalk, due to the physics of weakly coupled harmonic oscillators when tightly spaced in frequency.^{20,21} If this is not considered in the design, it can dominate all other forms of crosstalk (Fig. 2).

Consider the eigenmodes of two weakly coupled simple harmonic oscillators. At any frequency ω , the complex amplitudes x_1 and x_2 of the two oscillators must obey

$$\begin{bmatrix} k_1 - \omega^2 & k_c \\ k_c & k_2 - \omega^2 \end{bmatrix} \begin{bmatrix} x_1 \\ x_2 \end{bmatrix} = 0, \quad (1)$$

where k_1 and k_2 parameterize the spring constants of the two resonators and k_c parameterizes their coupling.

The excitable modes occur at frequencies

$$\omega^2 = \frac{k_1 + k_2}{2} \pm \frac{1}{2} \sqrt{(k_2 - k_1)^2 + 4k_c^2} \quad (2)$$

so that for $k_c \ll |k_2 - k_1|$, we can approximate

TABLE I. Simulated couplings between circuit elements of a NIST multiplexer design, in which resonators terminate at rf-SQUIDs in a zigzag manner. The columns consider couplings within one resonator, with its nearest neighbor, and with its next nearest neighbor. The rows describe the couplings responsible for direct inductive crosstalk, indirect inductive crosstalk, and coupled harmonic oscillator crosstalk.

M_{ij} (pH)	$(\Delta x, \Delta y)$ (μm)		
	(0, 0)	(250, -400)	(500, 0)
SQUID-Input	245	0.04 (0.02%)	<0.02 (0.01%)
Res.Term-SQUID	7.3	<0.01 (0.1%)	<0.002 (0.03%)
Res.Term.-Res.Term	97	0.05 (0.05%)	<0.01 (0.01%)

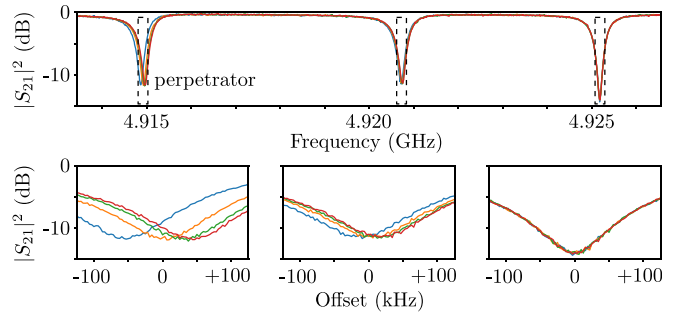


FIG. 2. Coupled harmonic oscillator crosstalk of one resonator into its nearest and next-nearest physical neighbor. The different curves result from different values of magnetic flux into the perpetrator channel. A failed design with 1-part-in-4 crosstalk into the nearest neighbor is shown for illustration purposes, but is not typical.

$$\omega_1^* \approx \sqrt{k_1 + \frac{k_c^2}{k_1 - k_2}}, \quad (3)$$

where ω_1^* denotes the actual resonance frequency associated with the first resonator, whose frequency without the coupling would be $\omega_1 = \sqrt{k_1}$.

In other words, the two resonances repel each other, hybridizing so that the eigenfrequency associated with each resonator depends slightly on the natural frequency of the other resonator. If the natural frequency of one resonator is perturbed, the other experiences a shift of

$$\chi = \frac{d\omega_1^*}{d\omega_2} = \frac{\omega_2}{\omega_1^*} \frac{k_c^2}{(\omega_1^* - \omega_2^*)^2}, \quad (4)$$

which, with a conversion of the circuit of Fig. 1 into the form of Eq. (1) and assuming relatively similar resonance frequencies $\bar{f} \approx f_1 \approx f_2$, becomes

$$\chi \approx \frac{16\bar{f}^4}{(f_2 - f_1)^2} \frac{M_x^2}{Z_0^2}, \quad (5)$$

where M_x is the mutual inductance between the resonators and Z_0 is their characteristic impedance.

This crosstalk mechanism therefore scales with the square of the coupling and inversely with the square of the frequency splitting. Crosstalk with precisely this behavior is observed in actual devices. Figure 2 shows a particularly bad example of coupled harmonic oscillator crosstalk, in which resonators placed closely in frequency space were also placed closely in physical space, allowing for a large parasitic mutual inductance.

To suppress this crosstalk, we attempt to not only reduce the parasitic coupling between physically adjacent resonators but also distribute resonances on a chip as shown in Fig. 3 such that physically adjacent resonators are far apart in frequency space and frequency adjacent resonators are far apart in physical space.^{20,21}

For example, the coupling between two quadrupole gradiometers falls off steeply with separation, as r^{-5} without a ground plane, and somewhat less steeply with screening currents in a ground plane. Thus, doubling the distance between a pair of frequency-adjacent resonators can reduce crosstalk between them by multiple orders of magnitude. Replacing that adjacent resonator by one at, for example,

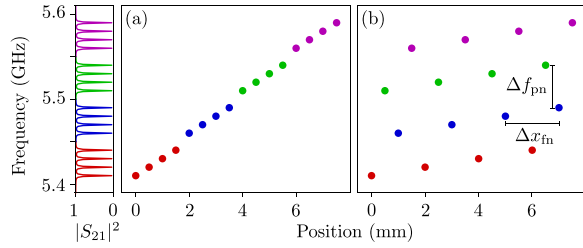


FIG. 3. Illustration of (a) monotonic and (b) interleaved resonator placement. Interleaving resonator subbands can separate frequency neighbors in physical space, Δx_{fm} , and physical neighbors in frequency space, Δf_{fm} .

32-fold frequency spacing increases crosstalk to the new resonator but leaves it at 10^{-3} of the original pair. We employ an interleaving pattern like this in all microwave SQUID multiplexers, reducing this form of crosstalk below the other forms of crosstalk discussed in this Letter.

A third mechanism of crosstalk results from the imperfect linearity of broadband microwave components in the system [Fig. 1(c)]. The nonlinearity of these components, which act on the superposition of microwave tones, results in weak mixing of the tones.

We model the nonlinearity of a broadband device in the readout chain as a Taylor expansion

$$V_{out} = GV_{in} + G_2 V_{in}^2 + G_3 V_{in}^3 + \dots \quad (6)$$

$$= G \left[V_{in} + \sqrt{\frac{2}{Z_0 IIP2}} V_{in}^2 + \frac{2}{3Z_0 IIP3} V_{in}^3 + \dots \right], \quad (7)$$

where G is the linear gain, Z_0 is the input impedance, and IIP3 (IIP2) is the input-referred 3rd-order (2nd-order) intercept point, a standard measurement of component nonlinearity by extrapolating the power in the intermodulation products, which scale as the cube (square) of input power, until they intercept the power in the signal.²² IIP3 typically scales with the input compression point.

Consider two carriers, a victim and a perpetrator with modulation tones to either side, presenting frequencies ω_1 , ω_2 , and $\omega_2 \pm \omega_m$ to the broadband device. The 2nd-order intermodulation products appear out of band, but the 3rd-order intermodulation products will appear as spurious sideband images around the victim at $\omega_1 \pm \omega_m$ as shown in Fig. 4. Substituting the superposition of carrier tones and modulation of sideband tones into the transfer function [Eq. (7)], one can show that the fractional crosstalk is

$$\chi \approx 4 \frac{P_{perp}}{IIP3}, \quad (8)$$

where P_{perp} is the power in the perpetrator tone at the input to the broadband component and the approximation allows for a difference between the modulation sidebands. This crosstalk therefore scales with the ratio of carrier power to IIP3. When we measure the crosstalk between resonators far apart in both frequency and physical space, we see this power dependence (Fig. 5).

Other mechanisms fall off with the physical distance and frequency separation, but this process sets a crosstalk floor, although at a relatively low level. Depending on the application, this weak all-into-all crosstalk can be more damaging than the stronger crosstalk that occurs between only spatial and frequency neighbors.

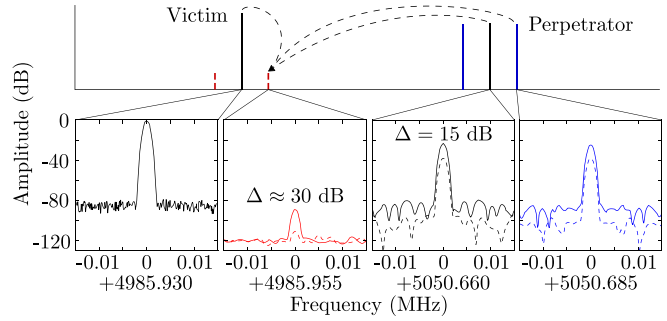


FIG. 4. Cartoon (top) showing how three-wave mixing can transfer modulation sideband tones from one carrier to another. Data (bottom) show how the amplitude of the crosstalk tone depends sensitively on the perpetrator power, with the solid and dashed lines representing a -15 dB difference.

Intermodulation crosstalk can be reduced, first by selecting broadband components with higher IIP3, second by interrogating the multiplexer with weaker probe tones and improving crosstalk at the cost of a slight increase in readout noise, and potentially third by utilizing a tone-tracking readout²³ that continually drives the probe tone to the deepest part of the resonance, minimizing power incident on the broadband components. This last method of crosstalk reduction is still unproven.

In the final crosstalk mechanism, we will examine results from the long tails of the Lorentzian resonance shapes as each resonator slightly affects transmission at frequencies far off resonance [Fig. 1(d)]. This is an unavoidable mechanism of crosstalk in the system and generally sets the minimum frequency spacing between resonances.

Consider two resonances, at f_1 and f_2 , coupled at different locations to the same feedline, measured at a fixed frequency f . Allowing for multiple reflections between them and ignoring an overall phase factor, we can write

$$S_{21} = \frac{(1 + \Gamma_1)(1 + \Gamma_2)}{1 - \Gamma_1 \Gamma_2 e^{2i\theta}}, \quad (9)$$

with

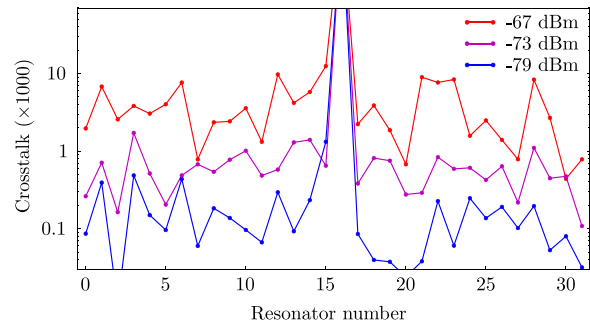


FIG. 5. Power dependence of end-to-end crosstalk measured in a microwave SQUID multiplexer. The broad crosstalk floor between distant resonators scales linearly with carrier power. Resonator 16 is the perpetrator channel. Resonator 15, the physical nearest neighbor, retains 0.1% crosstalk even at low power (due to frequency interleaving, resonator 17 is on the other side of the chip).

$$\Gamma_n \approx \frac{1}{-1 + i \frac{f - f_n}{BW/2}}, \quad (10)$$

where θ is the accumulated phase of a wave propagating between the two coupling locations and Γ_1 and Γ_2 are the reflectance of each resonator. For insight into the scaling of this crosstalk, consider the special case of $e^{2i\theta} = 1$, in which the above equation simplifies to

$$\frac{1}{S_{21}} \approx 1 + i \frac{BW}{2} \left[\frac{1}{f - f_1} + \frac{1}{f - f_2} \right], \quad (11)$$

and differentiate to obtain

$$\chi \approx \frac{\partial S_{21}}{\partial(f_2/BW)} \approx -\frac{i S_{21}^2}{2 n^2}, \quad (12)$$

where $n \equiv (f_2 - f_1)/BW$ is the number of bandwidths between the two resonances. This simplification illustrates the $1/n^2$ dependence of Lorentzian crosstalk on the frequency separation between resonators and the suppression of crosstalk when the probe tone is on resonance with the victim resonator. Real devices exhibit a more complicated flux-dependence (Fig. 6) that is qualitatively, although not exactly, predicted by a nontrivial phase delay on the feedline.

In order to maintain crosstalk between frequency adjacent resonators below 0.1%, it is therefore common to space resonances by roughly 10 times their bandwidth. Combined with the bandwidth necessary for each application, this criterion determines the number of channels that can be multiplexed in a given readout bandwidth.

The mechanisms discussed above all pertain to crosstalk between the microwave resonators or tones used to interrogate them. However, in all systems currently reading out microwave SQUID multiplexers, the SQUIDs are modulated²⁴ for reasons of linearization and noise mitigation, encoding the signal in the phase of the periodic SQUID response. The crosstalk therefore acts between phase-modulated signals, presenting unusual behavior after demodulation,

$$\phi_1^* = \arcsin(\sin \phi_1 + \chi \sin \phi_2) \quad (13)$$

$$\approx \phi_1 + \chi \sin(\phi_2 - \phi_1). \quad (14)$$

A large signal in ϕ_2 therefore results in sinusoidal rather than linear crosstalk into ϕ_1 as shown in Fig. 7(a). This both limits the amplitude of crosstalk from large signals and makes compensation for it

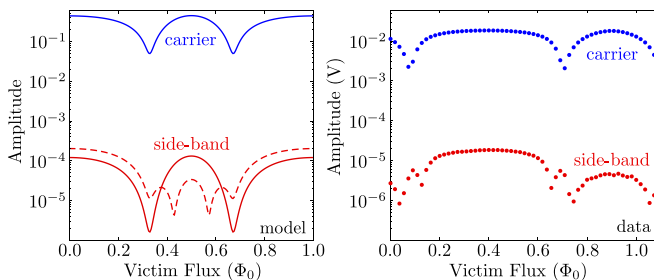


FIG. 6. Lorentzian crosstalk as a function of magnetic flux in the victim. Theory (left) shows the simple model with no distance between resonators on the feedline (red solid) and a more accurate model with the propagation phase between the resonators (red dashed). Actual data (right) show features roughly consistent with the physical placement of resonators on the feedline.

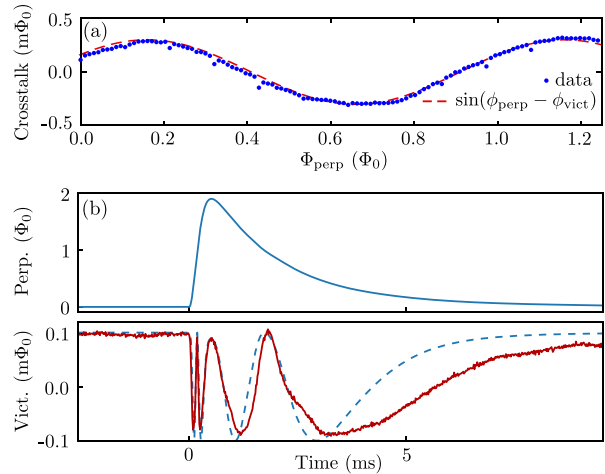


FIG. 7. (a) Sinusoidal behavior of crosstalk in the microwave SQUID multiplexer with flux-ramp modulation. (b) Theory and data showing the effect of this crosstalk behavior on a typical TES microcalorimeter pulse (the crosstalk pulse is contaminated by a slower signal).

more complex. It is hard to exactly model all crosstalk sources, and our understanding may still be incomplete, but observed crosstalk agrees qualitatively with this prediction [Fig. 7(b)].

In summary, the crosstalk is dominated by three major mechanisms: electromagnetic coupling between the resonators, nonlinear mixing in the broadband components, and the Lorentzian tails of the resonances. All three mechanisms can be mitigated in design, although the Lorentzian crosstalk ultimately constrains how closely resonances can be placed in frequency space. As a result of flux-ramp modulation, the apparent crosstalk is periodic, rather than linear. The amplitude of this crosstalk in a modern microwave SQUID multiplexer is low, typically below 1 m Φ_0 , but it is not negligible. Reduction of this crosstalk would improve the technology for applications ranging from precision cosmology, to x-ray metrology, to high-rate x-ray and γ -ray spectroscopy.

We are therefore continuing to work to reduce crosstalk, by reducing electromagnetic coupling between resonators, particularly those close in frequency, and by optimizing the readout chain to keep tone power consistently far below the IIP3 of the broadband components, and plan to test the effect of tone tracking on crosstalk.

The authors gratefully acknowledge the support of the U.S. DOE NEUP, NIST Innovations in Measurement Science, NASA SAT, and DOE BES ADR programs.

REFERENCES

¹K. Irwin, *Appl. Phys. Lett.* **66**, 1998 (1995).
²J. N. Ullom and D. A. Bennett, *Supercond. Sci. Technol.* **28**, 084003 (2015).
³D. A. Bennett, R. D. Horansky, D. R. Schmidt, A. Hoover, R. Winkler, B. K. Alpert, J. A. Beall, W. B. Doriese, J. W. Fowler, C. Fitzgerald *et al.*, *Rev. Sci. Instrum.* **83**, 093113 (2012).
⁴W. Doriese, K. Morgan, D. Bennett, E. Denison, C. Fitzgerald, J. Fowler, J. Gard, J. Hays-Wehle, G. Hilton, K. Irwin *et al.*, *J. Low Temp. Phys.* **184**, 389 (2016).
⁵H. Akamatsu, L. Gottardi, C. de Vries, J. Adams, S. Bandler, M. Bruijn, J. Chervenak, M. Eckart, F. Finkbeiner, J. Gao *et al.*, *J. Low Temp. Phys.* **184**, 436 (2016).

- ⁶K. Morgan, B. Alpert, D. Bennett, E. Denison, W. Doriese, J. Fowler, J. Gard, G. Hilton, K. Irwin, Y. Joe *et al.*, *Appl. Phys. Lett.* **109**, 112604 (2016).
- ⁷K. D. Irwin and K. W. Lehnert, *Appl. Phys. Lett.* **85**, 2107 (2004).
- ⁸J. A. B. Mates, "The microwave SQUID multiplexer," Ph.D. thesis, University of Colorado, 2011.
- ⁹J. Mates, G. Hilton, K. Irwin, L. Vale, and K. Lehnert, *Appl. Phys. Lett.* **92**, 023514 (2008).
- ¹⁰S. Kempf, M. Wegner, L. Gastaldo, A. Fleischmann, and C. Enss, *J. Low Temp. Phys.* **176**, 426 (2014).
- ¹¹F. Hirayama, S. Kohjiro, D. Fukuda, H. Yamamori, S. Nagasawa, and M. Hidaka, *IEEE Trans. Appl. Supercond.* **23**, 2500405 (2013).
- ¹²J. Mates, D. T. Becker, D. A. Bennett, B. Dober, J. Gard, J. Hays-Wehle, J. Fowler, G. Hilton, C. Reintsema, D. Schmidt *et al.*, *Appl. Phys. Lett.* **111**, 062601 (2017).
- ¹³M. Wegner, N. Karcher, O. Krömer, D. Richter, F. Ahrens, O. Sander, S. Kempf, M. Weber, and C. Enss, *J. Low Temp. Phys.* **193**, 462 (2018).
- ¹⁴Y. Nakashima, F. Hirayama, S. Kohjiro, H. Yamamori, S. Nagasawa, N. Y. Yamasaki, and K. Mitsuda, *IEICE Electron. Express* **14**, 20170271 (2017).
- ¹⁵B. Dober, D. T. Becker, D. A. Bennett, S. A. Bryan, S. M. Duff, J. D. Gard, J. P. Hays-Wehle, G. Hilton, J. Hubmayr, J. Mates *et al.*, *Appl. Phys. Lett.* **111**, 243510 (2017).
- ¹⁶S. Stanchfield, P. Ade, J. Aguirre, J. A. Brevik, H.-M. Cho, R. Datta, M. Devlin, S. R. Dicker, B. Dober, S. M. Duff *et al.*, in American Astronomical Society Meeting Abstracts (2018), Vol. 231.
- ¹⁷S. Kempf, M. Wegner, A. Fleischmann, L. Gastaldo, F. Herrmann, M. Papst, D. Richter, and C. Enss, *AIP Adv.* **7**, 015007 (2017).
- ¹⁸M. Faverzani, B. Alpert, D. Backer, D. Bennet, M. Biasotti, C. Brofferio, V. Ceriale, G. Ceruti, D. Corsini, P. Day *et al.*, *J. Low Temp. Phys.* **184**, 922 (2016).
- ¹⁹G. C. O'Neil, L. Miaja-Avila, Y. I. Joe, B. K. Alpert, M. Balasubramanian, D. Sagar, W. Doriese, J. W. Fowler, W. K. Fullagar, N. Chen *et al.*, *J. Phys. Chem. Lett.* **8**, 1099 (2017).
- ²⁰O. Noroozian, P. Day, B. Eom, H. Ledux, and J. Zmuidzinis, *IEEE Trans. Microwave Theory Tech.* **60**, 1235 (2012).
- ²¹F. Hirayama, T. Irimatsugawa, H. Yamamori, S. Kohjiro, A. Sato, S. Nagasawa, D. Fukuda, H. Sasaki, M. Hidaka, Y. Sato *et al.*, *IEEE Trans. Appl. Supercond.* **27**, 1 (2017).
- ²²See <https://www.maximintegrated.com/en/app-notes/index.mvp/id/5429> for "The IP3 Specification - Demystified" (accessed February 25, 2019).
- ²³S. W. Henderson, Z. Ahmed, J. Austermann, D. Becker, D. A. Bennett, D. Brown, S. Chaudhuri, H.-M. S. Cho, J. M. D'Ewart, B. Dober *et al.*, in *Millimeter, Submillimeter, and Far-Infrared Detectors and Instrumentation for Astronomy IX* (International Society for Optics and Photonics, 2018), Vol. 10708.
- ²⁴J. Mates, K. Irwin, L. Vale, G. Hilton, J. Gao, and K. Lehnert, *J. Low Temp. Phys.* **167**, 707 (2012).